Liquid Crystals
Publication details, including instructions for authors and subscription information:
http://www.informaworld.com/smpp/title~content=t713926090

Thermodynamic investigation of the thermotropic cubic mesogen, 1,2-bis(4- n -octyloxybenzoyl)hydrazine

Nobuyuki Morimoto

Online publication date: 06 August 2010

To cite this Article Morimoto, Nobuyuki(1999) 'Thermodynamic investigation of the thermotropic cubic mesogen, 1,2-bis(4- n -octyloxybenzoyl)hydrazine', Liquid Crystals, 26: 2, 219 — 228
To link to this Article: DOI: 10.1080/026782999205353
URL: http://dx.doi.org/10.1080/026782999205353

LIQUID CRYSTALS, 1999, VOL. 26, NO. 2, 219–228

Thermodynamic investigation of the thermotropic cubic mesogen, 1,2-bis(4-*n*-octyloxybenzoyl)hydrazine§

NOBUYUKI MORIMOTO†, KAZUYA SAITO†, YASUSHI MORITA‡, KAZUHIRO NAKASUJI‡ and MICHIO SORAI†*

†Microcalorimetry Research Center, School of Science, Osaka University, Toyonaka, Osaka 560-0043, Japan

‡Department of Chemistry, Graduate School of Science, Osaka University, Toyonaka, Osaka 560-0043, Japan

(*Received 6 July 1998; accepted 14 September 1998*)

The molar heat capacity of the thermotropic cubic mesogen 1,2-bis(4-*n*-alkoxybenzoyl)hydrazine, BABH(8) for short, with a purity of 99.43 mol % has been precisely measured with an adiabatic calorimeter at temperatures between 14 and 480 K. The enthalpy and entropy gained at each phase transition across the phase sequence of [crystal(2) → crystal(1) → cubic mesophase → SmC → isotropic liquid] have been determined. The existence of a solid-to-solid phase transition with a fairly large entropy change seems to be necessary for the alkyl moieties attached to both sides of the molecule to play the role of 'solvent' in the cubic mesophase. On the basis of curvature elasticity considerations, the small energy difference between the cubic and SmC phases is favourably accounted for in terms of the jointed-rod micelles model. The reason for the immiscibility of BABH(8) with the cubic D mesogen, 4′-*n*-hexadecyloxy-3′-nitrobiphenyl-4-carboxylic acid is discussed in terms of the large difference in their molecular size and of 'structure breaking' arising from the admixture of heterogeneously hydrogen-bonded materials.

1. Introduction

Thermotropic liquid crystals are usually characterized as optically anisotropic liquids. In fact, practical applications of liquid crystals are based on this anisotropic character. However, optically isotropic liquid crystals are well known in lyotropic systems, where spherical or rod micelles consisting of amphiphilic molecules form higher order cubic structures and solvent molecules (usually water) fill up the large interstices in the 'lattice'.

Quite interestingly, rare examples of optically isotropic phases have been reported even in thermotropic liquid crystal systems: one is in the 4′-*n*-alkoxy-3′-nitrobiphenyl-4-carboxylic acids [ANBC(*n*) for short: *n* being the number of carbon atoms in the alkoxy chain, *n* = 16, 18] found by Gray and his collaborators in 1957 [1] and the other is in the 1,2-bis(4-*n*-alkoxybenzoyl)hydrazines [BABH(*n*) for short: *n* = 8, 9, 10] reported by Demus and his collaborators in 1981 [2] (see figure 1). Demus *et al.* [3] designated the cubic mesophases of the ANBCs as smectic D in 1968, and on the basis of X-ray diffraction Diele *et al.* [4] suggested a body-centred-cubic structural model consisting of spherical micelles in 1972. From the analogy with lyotropic systems, Tardieu and Billard [5] proposed an interwoven, three dimensional jointed-rod micelles structures with overall cubic symmetry in 1976. Etherington *et al.* [6] claimed that since the smectic D phase is clearly established as having three dimensional periodicity and is definitely cubic, it should not be called a smectic phase, but simply the (cubic) D phase. On the

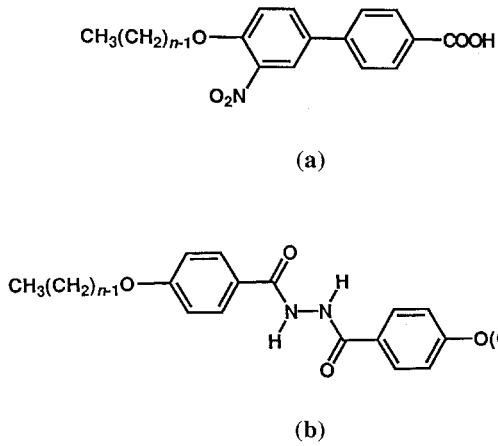

Figure 1. Molecular structures of thermotropic cubic mesogens: (*a*) 4′-*n*-alkoxy-3′-nitrobiphenyl-4-carboxylic acids, ANBC(*n*) for short; (*b*) 1,2-bis(4-*n*-alkoxybenzoyl)hydrazine, abbreviated as BABH(*n*).

*Author for correspondence.

§Contribution No. 149 from the Microcalorimetry Research Center.

other hand, since the D phases of the ANBCs appear at higher temperatures than the smectic C (SmC) phases, while the cubic phases of the BABHs occur at lower temperatures than the SmC phases, Demus *et al.* [2] regarded these two cubic mesophases as having different structures.

In spite of many structural investigations, no definite pictures have emerged concerning the higher order cubic structures formed by these non-amphiphilic molecules [7–9]. Although such liquid crystals seem to be far from practical usages, elucidation of their structures is basically important from the viewpoint of condensed states of matter.

Thermodynamic studies provide us with knowledge about the molecular motions closely related to a given structure. In order to elucidate the difference between these two mesomorphic cubic states from a thermodynamic viewpoint, we report here the first precise heat capacity measurements for BABH(8) based on adiabatic calorimetry.

2. Experimental

2.1. *Preparation of 1,2-bis(4-n-octyloxybenzoyl)-hydrazine*

The cubic mesogen 1,2-bis(3-*n*-octyloxybenzoyl)-hydrazine was synthesized by a condensation reaction between 4-*n*-octyloxybenzoyl chloride and hydrazine. Although Schubert *et al.* [10] carried out this reaction in an aqueous medium, we found that the yield is greatly improved when the reaction is carried out under non-aqueous conditions, in pyridine solution. The starting material 4-*n*-octyloxybenzoyl chloride, was prepared by heating under reflux a solution in benzene (100 ml) containing 0.1 mol of 4-*n*-octyloxybenzoic acid and 0.15 mol of thionyl chloride for 2 h. The excess of thionyl chloride and benzene was removed from the reaction solution by vacuum distillation. In 100 ml of pyridine cooled in an ice bath, 2.4 ml of hydrazine monohydrate was dissolved, and with stirring a solution of 0.5 equiv of 4-*n*-octyloxybenzoyl chloride was slowly added through a syringe. Then the solution was warmed to 70°C and stirred for 24 h. In order to remove the pyridine from the reaction solution, its pH was adjusted to 3 by adding ammonium chloride and 1M hydrochloric acid in a separatory funnel. By this treatment a large part of the pyridine was transferred to the aqueous layer. This procedure was repeated on the oily layer until almost all of the pyridine was removed. The oily fraction was finally dried under vacuum. The crude product was recrystallized four times from ethanol with addition of active charcoal. The final crystalline product was dried under high vacuum. The elemental analysis for the compound was in good agreement with the calculated values. Calc. for $C_{30}H_{44}O_4N_2$: C 72.55, H 8.93, N 5.64; found: C 72.45, H 8.96, N 5.66%. ^{1}H NMR and mass spectroscopy showed no contamination with by-products or unreacted materials. As described below, the purity of the compound was determined to be 99.43 mol % on the basis of the fractional melting method using the present adiabatic calorimeter.

2.2. *Physical methods*

Prior to heat capacity measurements, the thermal properties of the sample were preliminarily examined by using a differential scanning calorimeter (Perkin-Elmer, model DSC-7). The optical textures of the mesophases of BABH(8) were observed using a polarizing microscope (Olympus, model BHA-751-P) equipped with a heating stage (Union Optical Co., Ltd, model CMS-2).

Heat capacities were measured with an adiabatic calorimeter [11] in the 14–480 K range by using a sample cell having an inner volume of 10 cm^3. Since the sample cell of the calorimeter is made of gold-plated beryllium-copper alloy and oxygen-free copper, there is a risk of partial decomposition of the compound owing to direct contact between the specimen and the metal surfaces for a long period at high temperatures during heat capacity measurements. We therefore put a thin-walled quartz glass beaker with a lid inside the cell, whose mass is 5.6700 g. The calorimeter cell improved in this way contained 3.6359 g (equivalent to 7.3203 mmol) of BABH(8) after buoyancy correction using a density of 1.14 g cm^{-3} [2]. A small amount of helium gas was sealed in the cell to aid heat transfer. The temperature scale is based on IPTS-68.

3. Results

Figure 2 illustrates the heating and cooling DSC runs recorded at a scan rate of 10 K min^{-1}. As reported by Demus *et al.* [2], BABH(8) exhibited a solid-to-solid

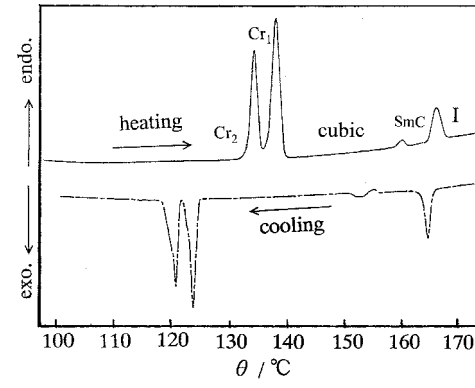

Figure 2. Heating and cooling DSC runs at a scan rate of 10 K min^{-1} for BABH(8). In this and in subsequent figures, the labels Cr_2, Cr_1, cubic, SmC and I stand for two crystalline phases, cubic mesophase, smectic C, and isotropic liquid, respectively.

phase transition just below the melting temperature. The high and low temperature crystalline phases will be designated hereafter as Cr_1 and Cr_2, respectively. The phase sequence $Cr_2 \rightarrow Cr_1 \rightarrow$ cubic $\rightarrow$ SmC $\rightarrow$ I on going from low to high temperatures was confirmed by observations by polarizing microscopy: at the phase transition between the cubic and SmC phases, well defined rectangular shapes of completely black areas characteristic of the cubic mesophase [3] coexisted with the birefringent schlieren texture of SmC. On a cooling run, the transition between the cubic and SmC phases considerably undercooled. This behaviour is quite rare in comparison with phase transitions occurring between usual anisotropic liquid crystalline states [2], implying that it is a characteristic feature of the cubic mesophase. Another remarkable observation, though not always occurring, is the existence of a small endothermic anomaly appearing just before the transition to the cubic phase, as seen in the cooling run of figure 2. This implies the possible existence of a metastable mesophase, which is energetically almost equivalent, but is entropically smaller than the cubic mesophase. A very clear endothermic behaviour on cooling has been reported by Yoshizawa *et al.* [12] for the transition from the chiral SmC to isotropic liquid phase in 2-{4-[(*R*)-2-fluorohexyloxy]-phenyl}-5-{4-[(*S*)-2-fluoro-2-methyldecanoyloxy]phenyl}-pyrimidine and its homologues.

Calorimetry was carried out in four series of observations and the results were evaluated in terms of molar heat capacities at constant pressure, C_p. Correction for vaporization of a sample in the liquid state into the free space of the calorimeter cell should be made. However, since the vapour pressure of the material under study seemed to be very small at the temperatures of the experiments and the free space of the cell (4.7 cm^3) was also small, we did not make this correction.

The measured molar heat capacities of BABH(8) are listed in table 1 and plotted in figure 3. As seen in the figure, there were no heat capacity anomalies below 400 K. In this temperature region the time required for thermal equilibration in the calorimeter cell after an electrical energy input for the heat capacity measurement was typically 20 min, which is basically the relaxation time of the cell itself. On the other hand, there were four temperature regions above 400 K, in each of which the thermal relaxation time became long owing to a phase transition. The first was the 405–406 K range for the $Cr_2 \rightarrow Cr_1$ phase transition. The thermal relaxation time was extremely long (several hours). To avoid undesirable extrapolation errors arising from such a long relaxation time, we stopped recording the temperature drift 2 h after the energy supply in this temperature region and regarded the temperature finally recorded as an 'equilibrium' value. Therefore, the absolute values of the heat capacities

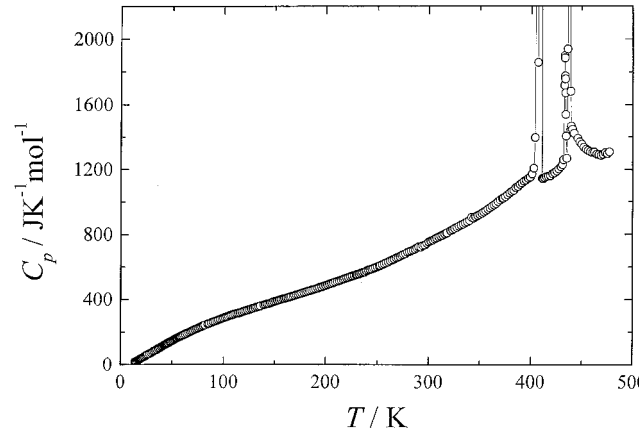

Figure 3. Molar heat capacities of BABH(8) in the entire temperature range of the present study. Open circles indicate the observed values, while the solid curves are drawn only as guides for the eye.

in the 405–406 K range involve rather large error bars, although the enthalpy increment through the phase transition has been determined accurately. In the remaining three regions, the relaxation time was 100 min (409–411 K; the $Cr_1 \rightarrow$ cubic transition), 50 min (433–434 K; the cubic $\rightarrow$ SmC transition), and 120 min (436–439 K; the SmC $\rightarrow$ I transition).

In order to compare the shapes and also the relative magnitudes of these four phase transitional features, the heat capacity peaks are shown in figures 4 and 5 with expanded temperature scales. The transition temperatures for the phase sequence $Cr_2 \rightarrow Cr_1 \rightarrow$ cubic $\rightarrow$ SmC $\rightarrow$ I, determined as the temperatures at which the heat capacities reach maximum values, were 405.20, 410.58, 433.27, and 437.51 K. These values compare well with 405.4, 409.9, 434.2, and 438.2 K obtained from DSC measurements by Demus *et al.* [2]. Two remarkable features are apparent in figures 4 and 5: one is the existence of a large enthalpy for the phase transition

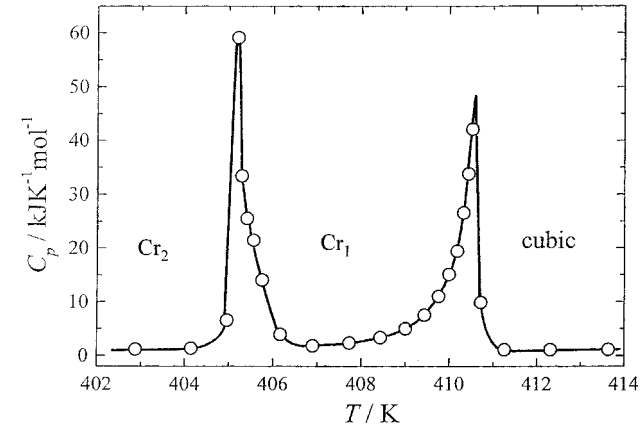

Figure 4. Molar heat capacities of BABH(8) in the range 402–414 K.

Table 1. Molar heat capacities of 1,2-bis(4-*n*-octyloxybenzoyl)hydrazine (M = 496.6904 g mol^{-1}).

T/K	C_p/J K^{-1} mol^{-1}	T/K	C_p/J K^{-1} mol^{-1}	T/K	C_p/J K^{-1} mol^{-1}	T/K	C_p/J K^{-1} mol^{-1}
Series 1		188.213	462.07	305.810	772.47	44.366	126.64
82.521	244.86	190.180	465.90	307.766	779.01	45.418	130.49
84.362	249.47	192.137	470.13	309.715	785.35	46.552	134.57
86.162	253.53	194.084	474.58	311.657	790.88	47.764	139.21
87.963	258.19	196.020	478.66	313.594	796.58	48.927	143.25
89.764	262.55	197.948	483.15	315.524	802.67	50.166	147.59
91.532	266.67	199.866	486.78	317.451	809.65	51.476	152.18
93.269	270.76	201.774	490.98	321.288	822.97	52.760	156.50
94.977	274.93	203.674	495.35	323.196	829.51	54.022	160.63
96.658	279.12	205.565	499.26	325.099	836.49	55.241	164.66
98.314	282.79	207.447	503.44			56.422	168.25
99.946	287.18	209.321	507.87	*Series 2*		57.568	171.97
101.556	290.96	211.187	511.90	214.111	518.12	58.683	175.42
103.146	294.74	213.044	515.69	215.959	524.38	59.889	178.85
104.716	298.26	214.895	519.72	217.798	525.93	61.243	183.20
106.267	302.63	216.738	524.20	219.632	529.28	62.786	187.66
107.800	305.51	218.573	528.12	221.457	534.15	64.448	192.64
109.317	308.13	220.401	532.31	223.276	538.69	66.057	197.46
110.975	311.37	222.221	536.33	225.087	542.01	67.619	202.01
112.772	314.28	224.034	540.83	226.892	546.19	69.137	206.44
114.547	317.19	225.840	544.74	228.690	549.23	70.617	210.85
116.301	320.05	227.639	547.96	230.481	554.40	72.201	215.63
118.036	324.22	229.431	552.03	232.265	557.29	73.886	220.54
119.834	327.45	231.216	557.20	234.042	562.40	75.529	225.17
121.693	331.43	232.993	565.81	235.813	565.71	77.133	229.72
123.533	334.98	234.767	568.04	237.579	569.41	78.702	233.88
125.354	338.62	236.533	568.29	239.337	576.71	80.238	238.00
127.157	342.58	238.292	574.41	241.087	580.82	81.744	241.90
128.944	346.11	243.541	592.51	242.831	584.27	84.671	249.83
130.714	349.83	245.272	590.39	244.569	587.76	86.098	252.74
132.468	353.12	246.999	595.17	246.302	591.97		
134.208	356.86	248.837	598.87	248.028	596.25	*Series 4*	
135.934	359.92	250.787	604.17	249.750	601.12	311.055	785.19
139.344	366.90	252.729	608.99	251.465	605.72	313.177	794.90
141.030	370.15	254.664	614.68	253.174	610.85	315.291	801.77
142.703	373.42	256.592	620.07			317.397	809.01
144.365	374.96	258.512	625.10	*Series 3*		319.460	815.90
146.016	379.02	260.424	631.09	14.230	18.33	321.479	822.73
147.656	382.73	262.328	637.38	15.498	20.76	323.492	828.94
149.356	387.59	264.225	643.11	16.711	25.18	325.497	838.31
151.117	390.23	266.115	647.86	17.871	29.49	327.496	843.36
152.865	393.26	267.997	654.54	18.902	32.59	329.489	850.84
154.602	396.78	269.872	659.02	19.920	37.39	331.476	857.56
156.328	400.75	271.740	664.21	20.928	41.02	333.507	863.36
158.042	404.80	273.599	671.16	22.024	44.91	335.558	871.22
159.747	406.16	275.451	676.43	23.206	49.19	337.626	877.95
161.441	409.19	277.293	681.17	24.458	53.80	339.689	884.98
163.127	411.90	279.124	690.38	25.585	59.19	341.741	903.99
164.802	415.08	280.944	694.16	26.776	64.07	343.785	899.91
166.468	419.09	282.762	698.26	28.291	67.41	345.826	908.92
168.125	422.13	284.578	703.69	29.906	72.88	347.860	915.12
169.773	425.34	286.389	709.45	31.368	78.78	349.890	922.76
171.412	429.43	288.189	716.81	32.709	84.09	351.912	929.83
173.043	432.63	290.070	723.47	34.072	88.82	353.928	937.78
174.806	435.65	292.032	721.86	35.458	93.74	355.937	945.49
176.700	439.71	293.991	731.46	36.869	99.06	357.940	953.97
178.584	443.27	295.968	734.87	38.307	104.25	359.936	963.50
180.458	446.95	297.948	745.04	39.654	109.41	361.925	972.76
182.321	450.63	299.922	753.91	40.922	114.08	363.908	981.21
184.248	453.81	301.889	760.00	42.125	118.49	365.885	989.23
186.236	458.42	303.852	765.61	43.270	122.67	367.854	1000.7

Table 1. (*Continued.*)

T/K	C_p/J K^{-1} mol^{-1}	T/K	C_p/J K^{-1} mol^{-1}	T/K	C_p/J K^{-1} mol^{-1}
369.815	1011.4	409.001	5011.1	434.721	1404.5
371.064	1012.4	409.431	7524.8	435.404	1268.8
373.067	1022.6	409.751	11004.	436.182	1939.6
375.091	1031.1	409.989	15103.	436.903	4025.6
377.132	1042.5	410.170	19437.	437.354	5723.7
379.166	1053.0	410.315	26592.	437.671	5789.9
381.193	1063.5	410.428	33791.	438.019	4351.5
383.212	1069.8	410.518	42118.	438.445	3043.9
385.228	1085.7	410.710	9877.	438.992	1681.3
387.234	1093.4	411.256	1144.0	439.628	1466.7
389.234	1106.0	412.312	1141.6	440.809	1445.5
391.228	1115.4	413.635	1148.1	442.519	1421.1
393.214	1126.9	415.293	1154.7	445.914	1390.5
395.194	1133.8	417.321	1158.4	447.984	1368.5
397.193	1144.4	419.382	1161.0	450.061	1354.0
399.208	1151.2	421.436	1173.4	452.147	1336.0
401.215	1171.9	423.484	1179.8	454.238	1324.0
402.869	1206.6	425.525	1190.6	456.331	1316.4
404.144	1395.4	427.537	1202.6	458.427	1309.6
404.955	6591.5	429.518	1216.1	460.523	1304.2
405.198	59112.	431.151	1228.6	462.618	1306.0
405.282	33430.	432.182	1259.8	464.715	1293.9
405.404	25587.	432.914	1717.4	466.812	1290.9
405.552	14055.	433.330	1899.7	468.911	1286.8
405.747	14055.	433.476	1885.2	471.003	1294.0
406.160	3965.4	433.624	1775.6	473.083	1303.4
406.896	1857.4	433.775	1757.4	475.151	1297.0
407.723	2375.2	433.982	1671.3	477.213	1307.5
408.431	3377.9	434.249	1538.5		

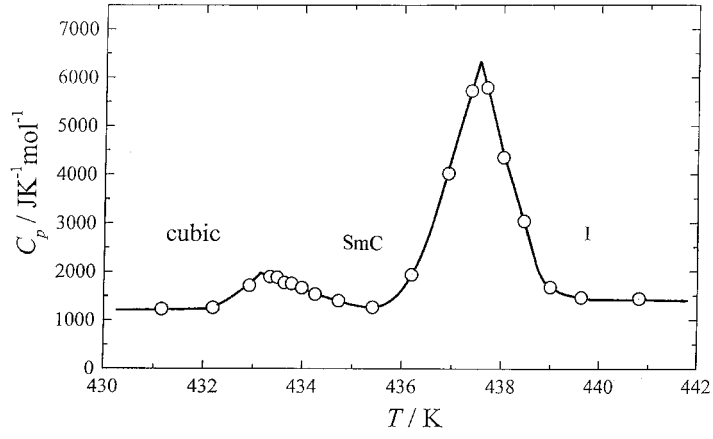

Figure 5. Molar heat capacities of BABH(8) in the range 430–442 K.

occurring in the solid state ($Cr_2 \rightarrow Cr_1$), comparable to that of the melting process ($Cr_1 \rightarrow$ cubic), and the other is the fact that the transition from cubic to SmC has a very small enthalpy. These four phase transitions are of first order as evidenced by the large thermal hysteresis revealed by DSC experiments.

In order to determine the excess thermodynamic quantities associated with each phase transition, we estimated the so-called normal heat capacity curves as follows. Since the phase transitions occur rather abruptly as shown in figure 3, we simply assumed either a linear or quadratic equation with temperature to represent the normal heat capacities. For example, the normal heat capacity for the crystalline state was determined by the least squares fitting of ten C_p points in the 380–400 K range to a formula, $C_p/\mathrm{J\,K^{-1}\,mol^{-1}} = a(T/\mathrm{K}) + b$, where the adjustable parameters were $a = 5.0404$ and $b = -857.77$. Similarly, the normal heat capacity was estimated to be $C_p/\mathrm{J\,K^{-1}\,mol^{-1}} = 0.13398\,(T/\mathrm{K})^2 - 108.70\,(T/\mathrm{K}) + 23\,186$ for the cubic and SmC phases

by using ten C_p points in the 412–430 K range, and $C_p/\mathrm{J\,K^{-1}\,mol^{-1}} = 2.1381\ (T/\mathrm{K}) + 286.30$ for the isotropic liquid phase on the basis of five C_p points in the 468–478 K range.

The base lines thus estimated are shown by dashed curves in figure 6. Strictly speaking, since all the phase transitions observed here are of first order, the baselines C_p should exhibit a discontinuous jump at each phase transition. However, it was impossible to determine independently the baseline C_p for the Cr_1 and SmC phases because of the narrow temperature intervals in which they are stable. The enthalpy $\Delta_{trs}H$ and entropy $\Delta_{trs}S$ at the phase transitions can be determined by integration of the excess heat capacities above the normal heat-capacity curves with respect to T and ln T, respectively. Table 2 summarizes the thermodynamic quantities associated with the phase transitions. The transition enthalpies determined from the present adiabatic calorimetry agree well with the DSC values obtained by Demus *et al.* [2]. The enthalpy and entropy gains through the four phase transitions are illustrated as a function of temperatures in figures 7 and 8,

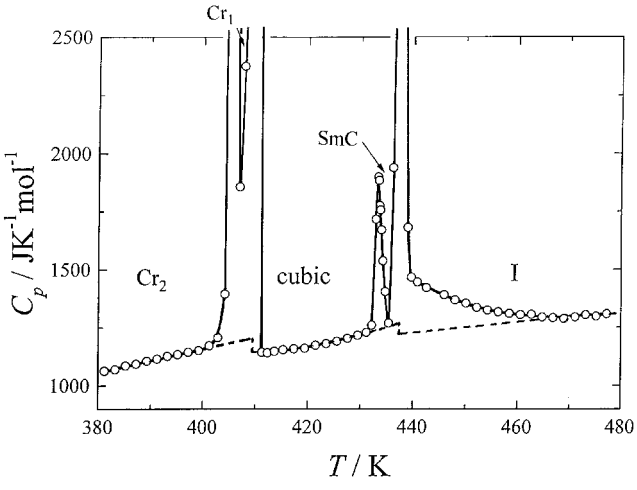

Figure 6. Molar heat capacities of BABH(8) in the range 380–480 K. The dashed curves represent the normal heat capacities.

Table 2. Thermodynamic quantities associated with the phase transitions of the cubic mesogen, 1,2-bis(4-*n*-octyloxybenzoyl)hydrazine.

Phase transition	T_{trs}/K	$\Delta_{trs}H$/ kJ mol^{-1}	$\Delta_{trs}S$/ J K^{-1} mol^{-1}
$Cr_2 \rightarrow Cr_1$	405.20	21.05	51.93
$Cr_1 \rightarrow$ cubic	410.58	27.60	67.33
cubic $\rightarrow$ SmC	433.27	0.98	2.26
SmC $\rightarrow$ I	437.51	9.97	22.66
Total		59.60	144.18

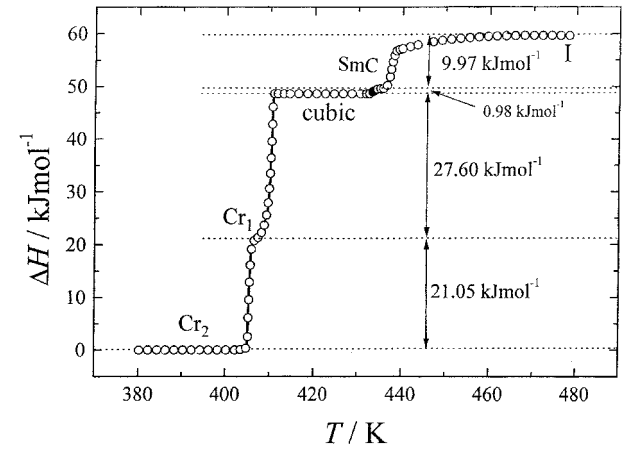

Figure 7. The enthalpy gain through the four phase transitions of BABH(8).

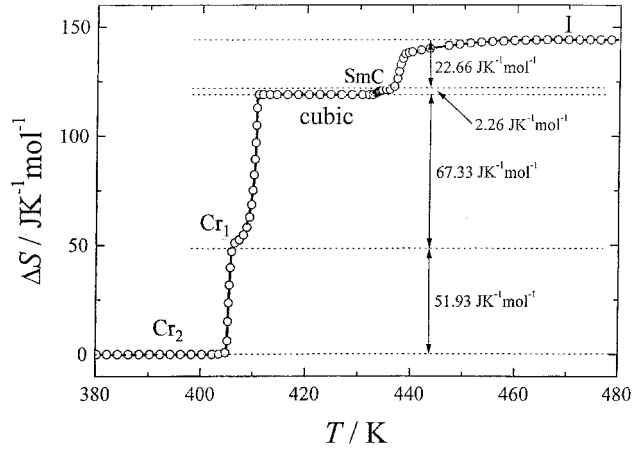

Figure 8. The entropy gain through the four phase transitions of BABH(8).

respectively. As mentioned above, the entropy change at the $Cr_2 \rightarrow Cr_1$ transition, $\Delta_{trs}S = 51.93\ \mathrm{J\,K^{-1}\,mol^{-1}}$, is very large, comparable to the melting entropy, $\Delta_{fus}S = 67.33\ \mathrm{J\,K^{-1}\,mol^{-1}}$. In contrast to this, the entropy gained at the cubic $\rightarrow$ SmC transition, $\Delta_{trs}S = 2.26\ \mathrm{J\,K^{-1}\,mol^{-1}}$, is extremely small, although the higher order structure of the molecular aggregation should be quite different in the cubic and SmC mesophases.

On the basis of the fractional melting method [13], the melting temperature of the virtually pure compound was estimated as 410.90 K and thereby the purity of the present specimen was determined to be 99.43 mol %. To derive the standard thermodynamic functions for the present compound, the heat capacities above 14 K were extrapolated to 0 K on the basis of the least squares fitting of the observed heat capacities in the 14–40 K range to a polynomial function of temperature: $C_p/\mathrm{J\,K^{-1}\,mol^{-1}} = a(T/\mathrm{K})^3 + b(T/\mathrm{K})^5 + c(T/\mathrm{K})^7 + d(T/\mathrm{K})^9$, where $a = 7.7975 \times 10^{-3}$, $b = -1.0010 \times 10^{-5}$,

$c = 6.1445 \times 10^{-9}$, and $d = -1.4161 \times 10^{-12}$. The standard molar heat capacity C_p°, molar entropy $S^\circ(T)$, enthalpy function $\{H^\circ(T) - H^\circ(0)\}/T$, and the Gibbs function $-\{G^\circ(T) - H^\circ(0)\}/T$ for BABH(8) at rounded temperatures are listed in table 3.

4. Discussion

As summarized in table 2, four phase transitions were observed in the present cubic mesogen BABH(8) at $T_{trs} = 405.20$ K ($Cr_2 \rightarrow Cr_1$), 410.58 K ($Cr_1 \rightarrow$ cubic), 433.27 K (cubic $\rightarrow$ SmC), and 437.51 K (SmC $\rightarrow$ I). The entropies gained at these phase transitions were $\Delta_{trs}S/J\,K^{-1}\,mol^{-1} = 51.93$, 67.33, 2.26, and 22.66, respectively. Of the total transition entropy of 144.18 $J\,K^{-1}\,mol^{-1}$, a large part (as much as 83%) is associated with the change from Cr_2 to the cubic mesophase, indicating that the cubic phase is actually a mesomorphic state. On the other hand, the entropy gained at the transition from the cubic mesophase to SmC is extremely small (only 2.26 $J\,K^{-1}\,mol^{-1}$). This suggests that although the aggregated states of the molecules in the cubic mesophase and the SmC phase should be quite different, there must exist a close resemblance between them from the viewpoint of entropy.

There seem to be two possible ways for rod-like molecules to form a phase having a high symmetry such as a cubic mesophase: in one, individual molecules undergo dynamic and random reorientation, eventually leading to high symmetry, and in the other, many molecules aggregate to form a higher order structure like micelles. The entropy gain up to the cubic mesophase is really large, but is still smaller than the value expected for full *gauche-trans*-type reorientational disordering of the constituent alkyl chains, as is shown later. Since this fact is unfavourable to the first possibility, it is very

Table 3. Standard thermodynamic functions for the cubic mesogen 1,2-bis(4-*n*-octyloxybenzoyl)hydrazine. The values in parentheses are calculated by extrapolation.

T/K	C_p°/ $J\,K^{-1}\,mol^{-1}$	$S^\circ(T)$/ $J\,K^{-1}\,mol^{-1}$	$\{H^\circ(T) - H^\circ(0)\}/T$/ $J\,K^{-1}\,mol^{-1}$	$-\{G^\circ(T) - H^\circ(0)\}/T$/ $J\,K^{-1}\,mol^{-1}$
5	(0.944)	(0.319)	(0.239)	(0.080)
10	(6.856)	(2.408)	(1.790)	(0.618)
20	37.486	15.449	11.198	4.251
30	73.266	37.672	26.162	11.510
40	110.69	63.927	42.652	21.275
50	147.01	92.553	59.918	32.635
60	179.21	122.29	77.199	45.093
70	209.02	152.18	93.915	58.262
80	237.37	181.98	110.12	71.860
90	263.10	211.44	125.71	85.733
100	287.31	240.40	140.64	99.758
120	327.81	296.56	168.64	127.92
140	368.17	350.15	194.28	155.86
160	406.61	401.86	218.46	183.40
180	446.06	452.00	241.54	210.47
200	487.08	501.08	263.99	237.08
220	531.40	549.57	286.28	263.29
240	578.27	597.70	308.55	289.16
260	629.77	645.90	331.16	314.74
280	692.21	694.79	354.65	340.14
298.15	745.95	739.82	376.73	363.09
300	754.15	744.46	379.03	365.43
320	818.50	795.15	404.47	390.69
340	887.87	846.80	430.80	416.00
360	963.81	899.64	458.24	441.40
380	1057.3	954.21	487.27	466.95
400	1159.4	1011.0	518.30	492.72
	Phase transition from Cr_2 to Cr_1 at 405.20 K			
	Phase transition from Cr_1 to cubic mesophase at 410.58 K			
420	1164.8	1187.3	665.12	522.20
	Phase transition from cubic mesophase to SmC at 433.27 K			
	Phase transition from SmC to isotropic liquid at 437.51 K			
440	1460.1	1263.4	709.53	553.84
460	1305.6	1323.9	737.89	586.04
470	1290.6	1351.8	749.76	602.04

likely that in the cubic mesophase the molecules form a higher order structure. Although the actual structure is unknown at present, the capability for hydrogen-bonding of the present mesogen could play an important role in forming a higher order aggregated structure in the cubic mesophase. Demus and his collaborators [2] proposed a cubic structure consisting of lattice units of spherical micellar dimensions ($a = 4.57$ nm, $Z = 115$ at 413 K).

One can discuss the aggregated structure of molecules on the basis of elastic properties. As the present mesogen has no chirality and does not exhibit a nematic phase, one need not take into account the twist and bend deformations. Only the splay distortion contributes to the curvature elasticity. The curvature elastic energy per unit area (w) relative to the lowest energy state (uniform parallel alignment of the director) is written as follows [14]:

$$w = (k_{11}/2)(1/R_1 + 1/R_2)^2 + k_{24}/(R_1 R_2) \qquad (1)$$

where R_1 and R_2 are the radii of curvature of the surface in the zx and zy planes (z being the direction of the director), respectively, and k_{11} and k_{24} are the splay and the saddle–splay elastic constants, respectively. Since a lamellar structure as encountered in the SmC phase has zero curvature ($R_1 = R_2 = \infty$), the curvature elastic energy becomes

$$w \text{ (lamellar structure)} = 0 \qquad (2)$$

in accord with the definition. Contrary to this, the formation of spherical micelles requires curvature strain in three dimensions and hence for a sphere of radius R, the curvature elastic energy amounts to

$$w \text{ (spherical micelle)} = (2k_{11} + k_{24})(1/R^2). \qquad (3)$$

Another alternative to the cubic structure, which has been regarded as a good candidate for the structure in the cubic D phase, is the so-called jointed-rod model of Tardieu and Billard [5]. This was initially observed in soap–water and lipid–water systems and designated as phase Q^{230} [15–17]. The structure consists of two interwoven, unconnected networks of short columns (rod micelles), linked three by three in a coplanar fashion. Its space group is $Ia3d$. The saddle–splay distortion occurs in this structure because of $R_1 = -R_2$. If this jointed-rod structure were formed in the present cubic phase, the curvature elastic energy would be given by the following equation ($|R_1| = |R_2| = R$)

$$w \text{ (jointed-rod micelle)} = -k_{24}(1/R^2). \qquad (4)$$

Obviously the splay distortion energy for the jointed-rod micelles structure is much smaller than that for the spherical micelles structure. Therefore the small enthalpy difference between the cubic and SmC phases in BABH(8) implies that the cubic structure might be accounted for in terms of the jointed-rod micelles model.

On the other hand, both the spherical micelles model of Diele *et al.* [4] and the jointed-rod micelles model of Tardieu and Billard [5] have been proposed for the ANBC(n) homologues. Although these models were initially proposed on the basis of X-ray diffraction analyses, no definite conclusions were reached owing to uncertainty in indexing poor powder diffraction data. However, dynamic viscoelastic properties [18], IR spectroscopy [19], and ^{14}N NMR [20] by Kutsumizu, Yano and their collaborators, and time-resolved diffraction experiments by Levelut and Clerc [21] support the jointed-rod micelles model. Since the cubic phase of BABH(8) does not exhibit complete miscibility with the cubic D phase of ANBC(16), Demus *et al.* [2] concluded that these two cubic phases are of different kinds. As discussed above however, the elastic energy consideration suggests that the cubic phase of BABH(8) could have a jointed-rod structure similar to that of ANBC. One of the reasons responsible for the immiscibility could originate in the large difference in molecular size between BABH and ANBC. The ANBC(16) molecule contains 16 carbon atoms in its alkoxy terminal chain. Since a dimer is formed through the carboxyl groups; the total number of carbon atoms in both end chains amounts to 32, whereas it is only 16 in the case of BABH(8). This large difference in the 'molecular' lengths could prevent the two cubic phases from giving complete miscibility. An alternative reason for the immiscibility could arise from 'structure breaking' which develops from the admixture of heterogeneously hydrogen-bonded systems. In the case of ANBC, intermolecular hydrogen bonds through the carboxyl groups bring about the formation of dimers [19], while in the case of BABH there is a strong tendency to the formation of hydrogen bonds between the CO and NH groups, leading to lateral interactions.

Since many classical nematogenic or smectogenic mesogens do not exhibit phase transitions with large C_p peaks within the solid state [22], the phase transition with a large entropy gain found for BABH(8) may be a characteristic feature of cubic mesogens. It should be remarked here that transitions within the solid state with large C_p peaks are found to be a necessary condition for the formation of columnar mesophases [22–27]. Phase transitions occurring within the solid state are mainly associated with successively increasing conformational disorder in alkyl chains attained through *gauche-trans*-type kinking [28], whereas melting is mainly concerned with positional and orientational disordering processes of a molecule as a whole. The entropy

gain for the *gauche-trans*-type reorientational disorder of the BABH(8) molecule can be given as follows [23]:

$$\begin{aligned}\Delta S\ (\text{side chains}) &= 14\Delta S(-CH_2-) + 2\Delta S(-CH_3) \\ &= (10.31 \times 14 + 3.78 \times 2)\ \text{J K}^{-1}\ \text{mol}^{-1} \\ &= 151.90\ \text{J K}^{-1}\ \text{mol}^{-1}. \qquad (5)\end{aligned}$$

The entropy gained at the transitions from crystal phase Cr_2 through to the cubic mesophase is $\Delta S(Cr_2 \rightarrow Cr_1) + \Delta S(Cr_1 \rightarrow \text{cubic}) = 119.26\ \text{J K}^{-1}\ \text{mol}^{-1}$. This is considerably smaller than the expected value for complete conformational disorder of the alkyl chains given by equation (5). However, the existence of solid-to-solid phase transitions associated with a sufficiently large entropy change seems to be a necessary condition for the appearance of the cubic mesophase, because the partial conformational melting of the alkyl moieties is favourable when the flexible alkyl chains play the role of 'solvent' in the cubic mesophase, as in the case of the actual solvent in lyotropic liquid crystals. In order to elucidate this role we have already examined the phase behaviour in binary systems consisting of ANBC(n) (n = 8, 16, 18) and n-tetradecane and obtained definite evidence for this role of the terminal chains [29, 30].

5. Concluding remarks

By precisely measuring heat capacities for the thermotropic cubic mesogen BABH(8) we have revealed two characteristic features: (1) the existence of a solid-to-solid phase transition with a fairly large entropy change, which would be necessary for the alkyl chains to play the role of 'solvent' in the cubic mesophase and (2) small enthalpy and entropy differences between the cubic and SmC phases, although the higher order structures of these mesomorphic states are quite different. On the basis of curvature elasticity considerations this small energy difference is consistent with the jointed-rod micelles model. It is of great interest to examine whether these features are also encountered in the cubic D mesogens. We are now carrying out heat capacity measurements for ANBC(16) [31–33] and ANBC(18) [34]. In order to obtain a better understanding of thermotropic cubic phases, we have also started calorimetric studies on lyotropic cubic mesophases [35].

Since the cubic D phase of ANBC(16) appears on the high temperature side of a SmC phase, while the cubic phase of BABH(8) is located on the low temperature side of a SmC phase, these two cubic mesophases have been regarded as being of different types [2]. However, their immiscibility could result from the large difference in the sizes of their molecules and from the 'structure breaking' arising from admixture of heterogeneously hydrogen-bonded materials. The best way to study the reasons for the immiscibility is to examine the phase diagram of a two-component system, in which the ANBC and BABH molecules have a similar length. If such a system shows complete miscibility between the two cubic mesophases, the importance of molecular size would be confirmed. On the other hand, if such a two-component system does not exhibit miscibility over the whole composition region, this could point to the importance of structure breaking.

One of the reasons why the aggregated structures of molecules in such cubic mesophases have not been elucidated is that, apart from ANBC and BABH, no thermotropic cubic mesogens have been reported for a long time. Recently, however, other candidates for the family of thermotropic cubic mesogens have been reported [9, 36–39]. Thermodynamic studies of these new mesogens will accelerate the understanding of this interesting aggregated state of matter.

We would like to express our sincere thanks to Emeritus Professor Koji Okano at the University of Tokyo for discussions concerning the elastic properties, and to Dr Yatsuhisa Nagano at Osaka University for the DSC measurements.

References

[1] Gray, G. W., Jones, B., and Marson, F., 1957, *J. Chem. Soc.*, 393.
[2] Demus, D., Gloza, A., Hartung, H., Hauser, A., Rapthel, I., and Wiegeleben, A., 1981, *Cryst. Res. Technol.*, **16,** 1445.
[3] Demus, D., Kunicke, G., Neelsen, J., and Sackmann, H., 1968, *Z. Naturforsch.*, **23a,** 84.
[4] Diele, S., Brand, P., and Sackmann, H., 1972, *Mol. Cryst. liq. Cryst.*, **17,** 163.
[5] Tardieu, A., and Billard, J., 1976, *J. Phys. (Paris)*, **37,** C3–79.
[6] Etherington, G., Leadbetter, A. J., Wang, X. J., Gray, G. W., and Tajbakhsh, A. R., 1986, *Liq. Cryst.*, **1,** 209.
[7] Demus, D., Diele, S., Grande, S., and Sackmann, H., 1983, *Advances in Liquid Crystals*, Vol. 6, edited by G. H. Brown (Academic Press), p. 1.
[8] Gray, G. W., and Goodby, J. W., 1984, *Smectic Liquid Crystals: Textures and Structures* (Leonard Hill), p. 68.
[9] Diele, S., and Göring, P., 1998, *Handbook of Liquid Crystals*, Vol. 2B, edited by D. Demus, J. W. Goodby, G. W. Gray, H.-W. Spiess, and V. Vill (Wiley-VCH), p. 887.
[10] Schubert, H., Hauschild, J., Demus, D., and Hoffmann, S., 1978, *Z. Chem.*, **18,** 256.
[11] Sorai, M., Kaji, K., and Kaneko, Y., 1992, *J. chem. Thermodyn.*, **24,** 167.
[12] Yoshizawa, A., Umezawa, J., Ise, N., Sato, R., Soeda, Y., Kusumoto, T., Sato, K., Hiyama, T., Takanishi, Y., and Takezoe, H., 1998, *Jpn. J. appl. Phys.*, **37,** L942.
[13] Mastrangelo, S. V. R., and Dornte, R. W., 1955, *J. Am. chem. Soc.*, **77,** 6200.

[14] DUNMUR, D., and TORIYAMA, K., 1998, *Handbook of Liquid Crystals*, Vol. 1, edited by D. Demus, J. W. Goodby, G. W. Gray, H.-W. Spiess, and V. Vill (Wiley-VCH), p. 253.
[15] LUZZATI, V., and SPEGT, P. A., 1967, *Nature*, **215,** 701.
[16] TARDIEU, A., and LUZZATI, V., 1970, *Biochim. Biophys. Acta*, **219,** 11.
[17] MARIANI, P., LUZZATI, V., and DELACROIX, H., 1988, *J. mol. Biol.*, **204,** 165.
[18] YAMAGUCHI, T., YAMADA, M., KUTSUMIZU, S., and YANO, S., 1995, *Chem. Phys. Lett.*, **240,** 105.
[19] KUTSUMIZU, S., KATO, R., YAMADA, M., and YANO, S., 1997, *J. phys. Chem. B*, **101,** 10666.
[20] TANSHO, M., ONODA, Y., KATO, R., KUTSUMIZU, S., and YANO, S., 1998, *Liq. Cryst.*, **24,** 525.
[21] LEVELUT, A.-M., and CLERC, M., 1998, *Liq. Cryst.*, **24,** 105.
[22] SORAI, M., 1985, *Thermochim. Acta*, **88,** 1.
[23] SORAI, M., TSUJI, K., SUGA, H., and SEKI, S., 1980, *Mol. Cryst. liq. Cryst.*, **59,** 33.
[24] SORAI, M., and SUGA, H., 1981, *Mol. Cryst. liq. Cryst.*, **73,** 47.
[25] SORAI, M., YOSHIOKA, H., and SUGA, H., 1982, *Mol. Cryst. liq. Cryst.*, **84,** 39.
[26] VAN HECKE, G. R., KAJI, K., and SORAI, M., 1986, *Mol. Cryst. liq. Cryst.*, **136,** 197.
[27] SORAI, M., ASAHINA, S., DESTRADE, C., and NGUYEN, H. T., 1990, *Liq. Cryst.*, **7,** 163.
[28] BLASENBREY, S., and PECHHOLD, W., 1967, *Rheologica Acta*, **6,** 174.
[29] SAITO, K., SATO, A., and SORAI, M., 1998, *Liq. Cryst.*, **25,** 525.
[30] SAITO, K., SATO, A., MORIMOTO, N., YAMAMURA, Y., and SORAI, M., *Mol. Cryst. liq. Cryst.* (submitted).
[31] SATO, A., SAITO, K., and SORAI, M., 1997, in Proceedings of the 23rd Japanese Conference on Liquid Crystals, Tokyo, 1997, 3PD11.
[32] SATO, A., MORIMOTO, N., NAGANO, Y., SAITO, K., and SORAI, M., 1997, in Proceedings of the 33rd Japanese Conference on Calorimetry and Thermal Analysis, Okayama, 1997, 3B1000.
[33] SATO, A., SAITO, K., and SORAI, M., *Liq. Cryst.*, in press.
[34] SATO, A., YAMAMURA, Y., SAITO, K., and SORAI, M. (in preparation).
[35] NISHIZAWA, M., SAITO, K., and SORAI, M., unpublished results.
[36] YANO, S., MORI, Y., and KUTSUMIZU, S., 1991, *Liq. Cryst.*, **9,** 907.
[37] FISCHER, S., FISCHER, H., DIELE, S., PELZL, G., JANKOWSKI, K., SCHMIDT, R. R., and VILL, V., 1994, *Liq. Cryst.*, **17,** 855.
[38] WEISSFLOG, W., PELZL, G., LETKO, I., and DIELE, S., 1995, *Mol. Cryst. liq. Cryst.*, **260,** 157.
[39] WEISSFLOG, W., LETKO, I., PELZL, G., and DIELE, S., 1995, *Liq. Cryst.*, **18,** 867.